



PCCP

Origin of short- and medium-range order in supercooled liquid Ge₃Sb₂Te₆ from ab initio molecular dynamics simulations

Journal:	<i>Physical Chemistry Chemical Physics</i>
Manuscript ID	CP-ART-01-2020-000389.R1
Article Type:	Paper
Date Submitted by the Author:	25-Mar-2020
Complete List of Authors:	Qiao, Chong; Fudan University - Handan Campus Guo, Y. R. ; Fudan University - Handan Campus Wang, Songyou; Fudan University - Handan Campus Jia, Yu; Henan University, Key Laboratory for Special Functional Materials Wang, Cai Zhuang; Iowa State University Ho, Kai Ming; Iowa State University

SCHOLARONE™
Manuscripts

Origin of short- and medium-range order in supercooled liquid $\text{Ge}_3\text{Sb}_2\text{Te}_6$ from *ab initio* molecular dynamics simulations

Chong Qiao¹, Y. R. Guo¹, Songyou Wang^{1,2,*}, Yu Jia^{3,*}, Cai-Zhuang Wang⁴ and Kai-Ming Ho⁴

¹*Shanghai Ultra-Precision Optical Manufacturing Engineering Center and Department of Optical Science and Engineering, Fudan University, Shanghai, 200433, China*

²*Key Laboratory for Information Science of Electromagnetic Waves (MoE), Shanghai 200433, China*

³*Key Laboratory for Special Functional Materials of Ministry of Education and School of Materials Science and Engineering, Henan University, Kaifeng, Henan 475001, China*

⁴*Ames Laboratory, US Department of Energy and Department of Physics, Iowa State University, Ames, Iowa 50011, USA*

Corresponding Authors

***Email:** songyouwang@fudan.edu.cn; jiayu@henu.edu.cn

Abstract

Phase-change materials such as Ge-Sb-Te compounds have attracted much attention due to the potential value for electrical data storage. In contrast to the amorphous and crystalline phases, supercooled liquid is far from to be deeply understood despite of the inevitable role in both amorphization and crystallization process. To this end, we have studied the dynamics property and structural characteristic of liquid and supercooled liquid $\text{Ge}_3\text{Sb}_2\text{Te}_6$ during the fast cooling process. As the temperature decreases, chemical bonds become more homogeneous, but coordination numbers of Ge, Sb and Te atoms change very little. Meanwhile, the structural order of short-range configuration is obvious enhanced. Further studies suggest that Ge-centered, Sb-centered and Te-centered configurations change to the more ordered defective octahedrons mainly by adjusting the bond-angle relation and bond length, rather than

just changing the coordination environment. It is the more ordered octahedrons that promote the formation of medium-range order. Our findings provide a deep insight on the origin of local structural order in supercooled liquid $\text{Ge}_3\text{Sb}_2\text{Te}_6$, which are of great importance for the comprehensive understanding of amorphization and crystallization processes.

Keywords: phase-change material; supercooled liquid; short-range order; molecular dynamics

Introduction

The Ge-Sb-Te compounds located on pseudobinary line between Sb_2Te_3 and GeTe , as the typical phase-change materials (PCMs), possess a large potential for the non-volatile electronic memory due to the fast and reversible transformation between amorphous and crystalline phases with a large contrast in electrical resistivity¹⁻⁷. In one data-storage cycle, PCM is first melted and then fast cooled to a supercooled liquid and eventually to an amorphous state for the RESET operation, while the amorphous PCM is heated to a state above glass-transition temperature and held for tens of nano-seconds to crystallize for the SET operation. Compared to the amorphous⁸⁻¹² and crystalline¹³⁻¹⁸ phases of PCMs which have attracted a large amount of interests in the past decades, the supercooled liquid (the mother of amorphous and crystalline states) of PCM seems to be ignored with a few of researches¹⁹⁻²².

Compared with the well-known PCMs such as Sb_2Te_3 ²³⁻²⁵, GeSb_2Te_4 ²⁶⁻²⁸, $\text{Ge}_2\text{Sb}_2\text{Te}_5$ ²⁹⁻³¹ and GeTe ³²⁻³⁴, the sister $\text{Ge}_3\text{Sb}_2\text{Te}_6$ (GST326) seems to be desolated regardless of its good performance³⁵. Then we turn to study GST326 for further understanding of the phase-change mechanism in PCM. Previous studies revealed that GST326 also have two crystalline phases: a stable phase and a metastable phase³⁶⁻³⁸. The stable phase is a hexagonal structure with an ordered stacking of Ge-Te-Ge-Te-Sb-Te-Te-Sb-Te-Ge-Te³⁶. The metastable phase, which is usually used

for phase-change memory, is a rocksalt-like structure with an ABAB (A: Ge, Sb and vacancy, B: Te) alternation³⁷⁻³⁸. Our previous investigation found that the amorphous GST326 is composed of a large amount of defective octahedrons and a small portion of Ge-centered tetrahedrons¹². As metastable crystalline and amorphous GST326 are mainly composed of defective octahedrons, and both of them are formed from the supercooled liquid, it is expected that the supercooled liquid is the origin of structural order in PCM. Recently, Zalden et al. reported a liquid-liquid phase transition in the supercooled liquid stage of PCMs^{22, 39}, making the supercooled liquid of PCM even more amazing.

In the work, we have studied the dynamics property and short-range structural signature in liquid and supercooled liquid GST326 upon fast cooling, to explore the origin of structural order in PCMs by using *ab initio* molecular dynamics (AIMD) simulations. Our research results reveal that the local configurations in supercooled liquid GST326 inherit the coordination environment from the liquid. Nevertheless, the relative disordered short-range configurations begin to present the ordered octahedral characteristics. Then it is clear that the formation of short-range order (SRO) in supercooled liquid dominantly depends on the arrangement of bond-angle relation during the fast cooling process. In addition, medium-range order (MRO) is observed as the structural order of defective octahedron is enhanced, hinting that the enhancing structural order of defective octahedron is the origin of SRO and MRO in PCM. Our findings provide a deep insight on the origin of structural order in PCMs, which can promote the design and application of PCMs.

Methods

Using the VASP package based on the density functional theory⁴⁰⁻⁴¹, the AIMD simulations were performed to investigate the short-range structural characteristics in liquid and supercooled liquid GST326 upon fast cooling. The projector-augmented wave (PAW) method and Perdew-Burke-Ernzerhof generalized gradient approximation (GGA-PBE) were used for the exchange-correlation energy

functional⁴²⁻⁴³. The cutoff energies were set to 400 eV and 500 eV for AIMD simulation and calculation of electronic property, respectively. During the AIMD simulations, only one Γ point was chosen in the Brillouin zone, the canonical (NVT) ensemble was applied with a time step of 3 fs and the Nose-Hoover thermostat with an effective mass of 2 was utilized to control the temperature. The initial cubic cell consisted of 60 Ge, 40 Sb and 120 Te atoms. Same to our previous studies^{11-12, 20}, the simulation cell was firstly kept at 2000 K for 30 ps to eliminate the memory effect. Secondly, the system was cooled down to 1273 K and fully relaxed to obtain an equilibrium liquid. Then, the liquid was gradually cooled down to each sampled temperature (1123 K, 1023 K, 923 K, 823 K, 773 K) and eventually to 723 K with a cooling rate of 33.3 K/ps. During the cooling process, the system was adjusted to make the pressure tend to zero. The length of the cubic box varied from 20.12 Å to 19.84 Å as the temperature decreased from 1273 K to 723 K. For each sample, it was relaxed for 6000 steps to collect the atomic trajectories, and the final configuration was regarded as the beginning of the next cooling process. Finally, these trajectories were utilized to analyze the evolution of local configurations in the fast cooling process.

Results and discussion

Fig. 1(a) shows mean square displacement (MSD) of GST326 at different temperatures. MSD, as a common parameter to characterize the atomic mobility, is a function of time,

$$\langle R_{\alpha}^2(t) \rangle = \frac{1}{N_{\alpha}} \left\langle \sum_{i=1}^{N_{\alpha}} |R_{i\alpha}(t+\tau) - R_{i\alpha}(\tau)|^2 \right\rangle \quad (1)$$

where N_{α} is the number of α atoms, $R_{i\alpha}$ are the coordinates of atom i , and τ is the arbitrary origin of time. Then $\langle R_{\alpha}^2(t) \rangle$ represents the mean-squared distance over which the atoms have moved in the time interval t . From Fig. 1(a), all of the MSDs present a linear behavior with time. MSD decreases with the decreasing temperature, indicating that the atomic mobility is reduced in the fast cooling process. According to

the Einstein formula, diffusion coefficients (D) can be computed as follows:

$$D = \frac{1}{6} \frac{\partial}{\partial t} \lim_{t \rightarrow \infty} \langle R_{\alpha}^2(t) \rangle. \quad (2)$$

With the linear fitting to the MSD curves, the diffusion coefficients at different temperatures can be obtained. The standard errors are very small, with the values of $\sim 0.001 \text{ \AA}^2/\text{ps}$. In addition, it also follows the Arrhenius equation:

$$D = D_0 \exp\left(-\frac{E_{\alpha}}{k_B T}\right) \quad (3)$$

where D_0 represents the pre-exponential factor, E_{α} and k_B are the activation energy and Boltzmann constant, respectively. Fig. 1(b) plots the relation between $\ln D$ and $1/T$. By using a linear fitting, the pre-exponential factor D_0 and activation energy are obtained, with the values of $1.3 \times 10^{-7} \text{ m}^2/\text{s}$ and $0.28 \pm 0.01 \text{ eV}$, respectively. The linear relation between $\ln D$ and $1/T$ illustrates that the supercooled liquid GST326 at a high temperature shows a similar dynamics property to the liquid.

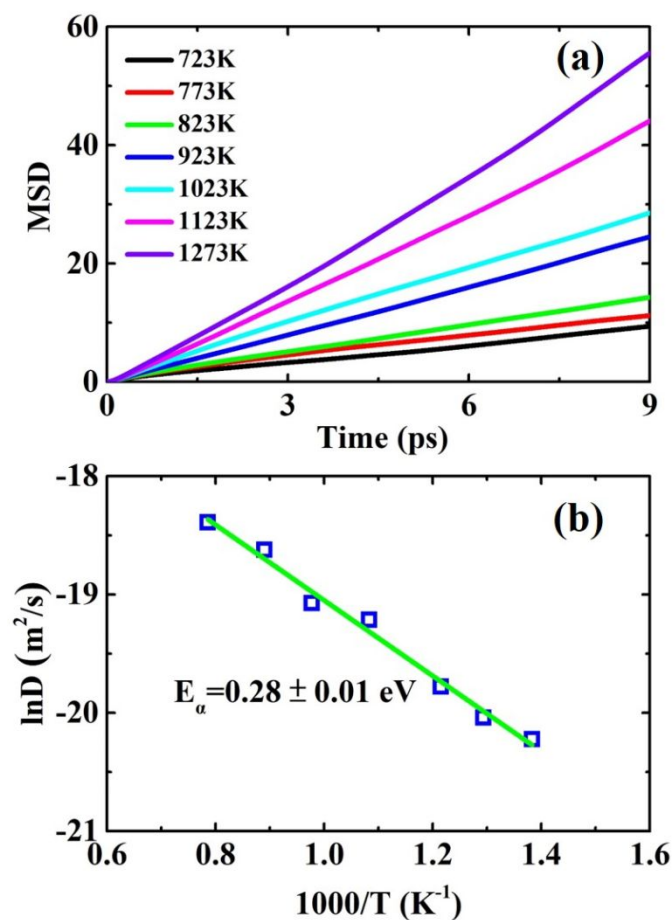


Fig. 1 (a) MSD and (b) diffusion coefficient D of GST326 at different temperatures.

Fig. 2 shows the total and partial pair correlation functions (PCFs) of GST326 during the fast cooling process. There is only one prominent peak (at ~ 2.9 Å) in the total PCFs as the temperature is above 923 K, illustrating that the liquid GST326 possesses a short-range structure. As the temperature decreases continuously, the liquid GST326 changes to a supercooled liquid (the melting temperature of GST326 is ~ 913 K⁴⁴ and the crystallization temperature is ~ 433 K⁴⁵), the notable peak in PCF becomes sharper and its amplitude becomes higher, hinting that the bond lengths in short-range configurations become homogeneous. Meanwhile, a slight peak at ~ 4.2 Å is observed, suggesting that MRO begins to be formed in the supercooled liquid. From the partial PCFs, the first peaks of Ge-Te and Sb-Te configurations are notable in liquid and become larger with the decreasing temperature, while the first peaks of Ge-Ge, Ge-Sb and Te-Te configurations are relative small at high temperature and reduce at a lower temperature. Interestingly, the first peak of Sb-Sb configuration changes little with the temperature. As for the MRO, the partial PCFs of Ge-Ge, Sb-Sb, Ge-Sb and Te-Te configurations present a second peak at the vicinity of 4.2 Å, in contrast to the first peaks, the second peaks increase gradually as the temperature decreases. At 723K, the second peak of Te-Te configuration is very large while the ones of other configurations are relative small. Then it is inferred that Te atoms play a significant role in the formation process of MRO.

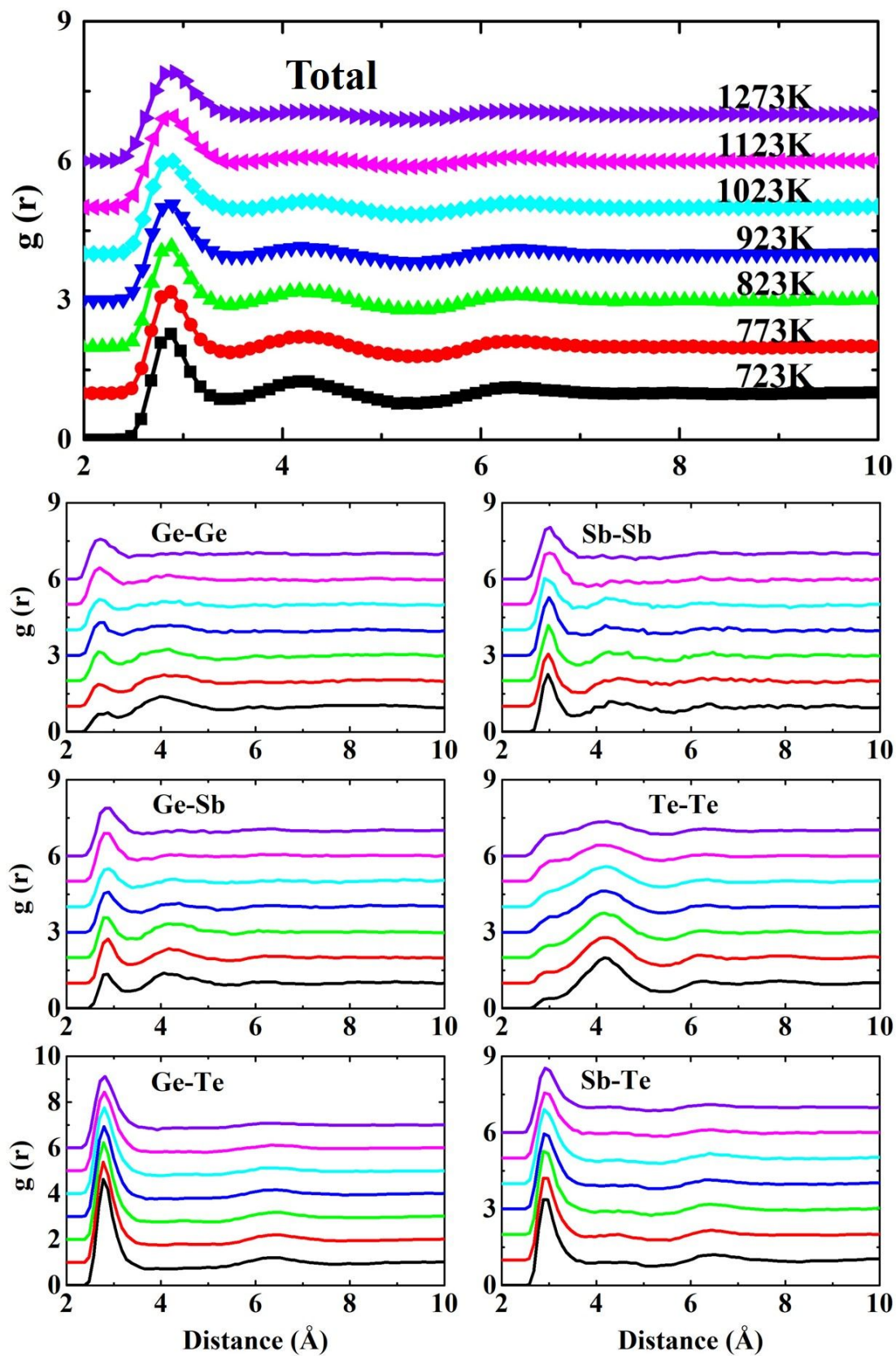


Fig. 2 Total and partial PCFs of GST326 at different temperatures.

The bond-angle distribution functions (BADFs) of Ge-centered, Sb-centered and Te-centered configurations in GST326 are shown in Fig. 3(a)-(c), respectively. In line with the previous literatures¹¹⁻¹², a cutoff radius of 3.2 Å is chosen to identify the bonding conditions. Similar to the cases in Sb₂Te₃²³, GeSb₂Te₄⁴⁶, Ge₂Sb₂Te₅⁸ and GeTe⁴⁷, the notable peaks also locate at the vicinity of 90°, indicating that local structures in liquid and supercooled liquid GST326 also present an octahedral characteristic. With a decrease in temperature, the amplitudes of the peaks are obviously increased, revealing that the disordered SROs tend to change to the ordered octahedral structures. In order to explore the extent of variation in Ge-centered, Sb-centered and Te-centered configurations, the width at half main peak in BADF is used as a function of temperature, as seen in Fig. 3(d). The three widths reduce notably as the temperature decreases, implying that the disordered configurations tend to form the more ordered clusters by adjusting the bond-angle relations. Interestingly that, the width of main peak for Ge-centered configurations decreases abruptly as the temperature is below 923 K, illustrating that Ge-centered structures are easier to form the ordered clusters during the supercooled liquid stage.

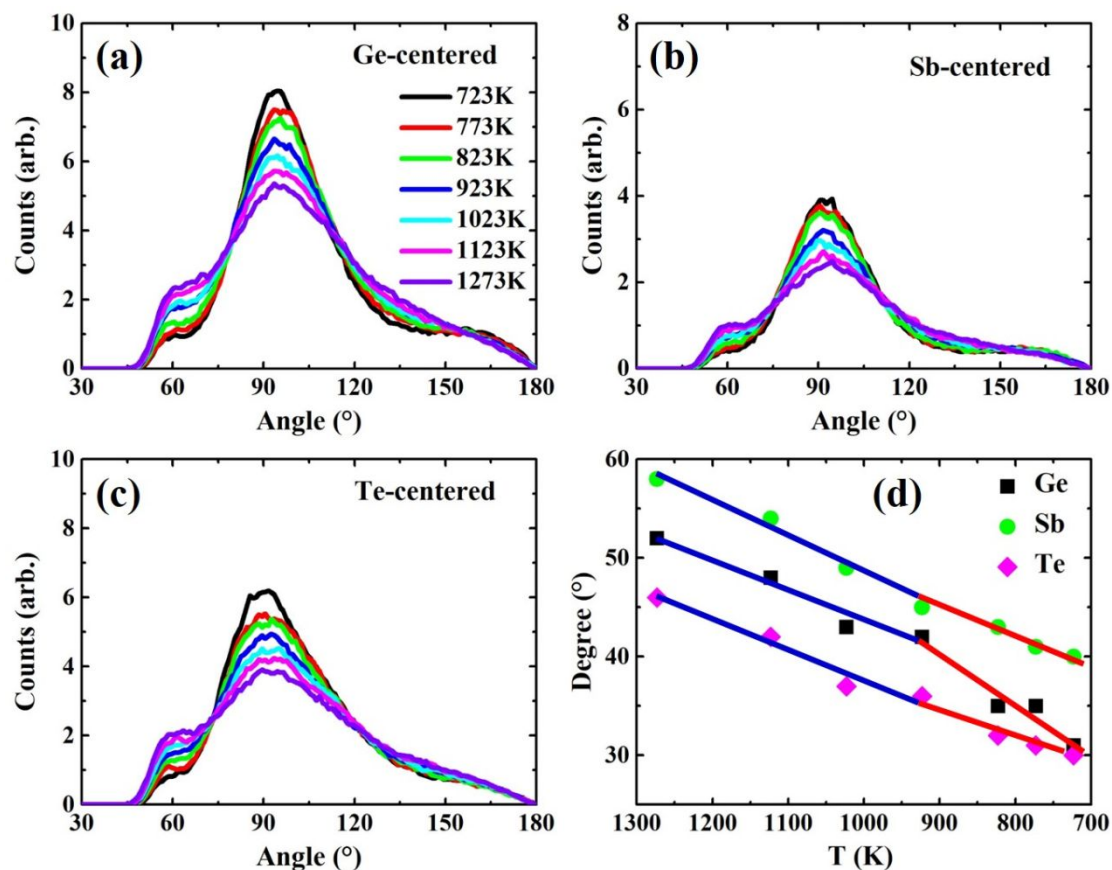


Fig. 3 BADFs of (a) Ge-centered, (b) Sb-centered and (c) Te-centered configurations in GST326 at different temperatures. (d) The width at half main peak in BADF as a function of temperature. The blue and red lines are the fitting lines above and below 923 K, respectively.

Coordination numbers (CNs) of Ge, Sb and Te atoms are shown in Fig. 4(a)-(c), respectively. Total CNs of Ge, Sb and Te atoms change very little with the decreasing temperature, however, the CNs of heteropolar bonds (Ge/Sb-Te) increase gradually while those of homopolar bonds (such as Ge-Ge, Ge-Sb and Te-Te) decrease during the fast cooling process. Then it is inferred that the clusters in supercooled liquid maintain the CNs from the liquid, but become more ordered by forming more heteropolar bonds. Fig. 4(d)-(f) present the distributions of CNs for Ge, Sb and Te atoms, respectively. For the Ge-centered configurations, the fraction of CN=2 decreases while the fraction of CN=4 increases as the temperature decreases. For the Sb-centered configurations, the fraction of CN=2 decreases while the fraction of CN=3 increases. As for Te-centered cases, the fraction of CN=1 decreases while the

fraction of CN=3 increases. It is clear that the relative disordered 1- and 2-dimensional (CN=1 and CN=2) configurations change to the 3-dimensional (CN=3 and CN=4) structures in the fast cooling process. Despite of the changes in distributions of CNs with temperature, CNs of Ge atoms always concentrate on 3 and 4, CNs of Sb atoms center on 3 while those of Te atoms concentrate on 2 and 3 during the whole cooling process. Compared to the notable change in BADF (as seen in Fig.3), variations in coordination environments are relatively small for the enhancement of structural order in the supercooled liquid.

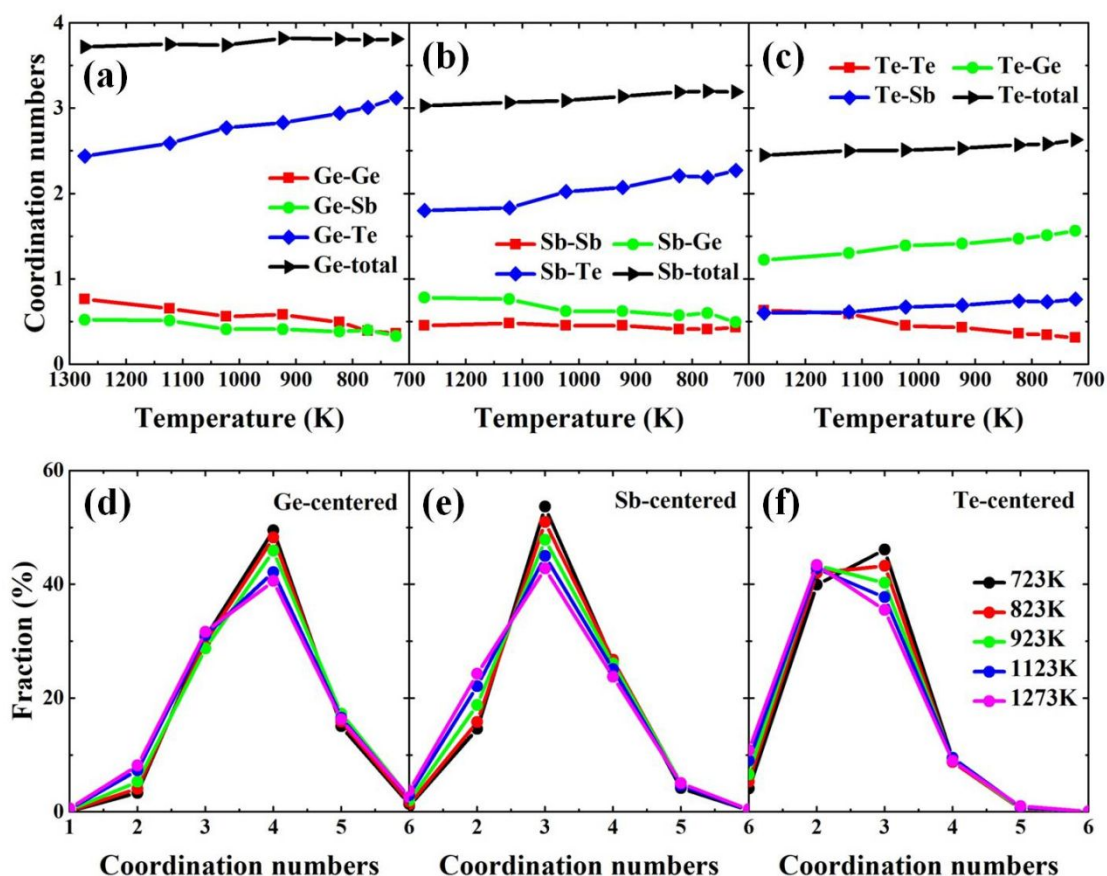


Fig. 4 CNs of (a) Ge, (b) Sb and (c) Te atoms at different temperatures. (d), (e) and (f) are the corresponding distributions of CNs for the three configurations, respectively.

To further explore evolutions of the SROs in GST326, collective alignment from an atomistic cluster alignment (ACA) method⁴⁸ is utilized to obtain the average local structures. Firstly, 2000 clusters consisted of one center atom and six nearest atoms

are randomly chosen from the atomic trajectories. Then, put the center atoms of these clusters to a same position, and then minimize the overall mean-square distances between different clusters by rigid rotation and relative translation. Finally, the average short-range structures are obtained and the corresponding atomic density contour plots with an isovalue of 0.2 \AA^{-3} are shown in Fig. 5. At 1273 K, the Ge-centered, Sb-centered and Te-centered configurations are relative disorder. While the Ge-centered and Sb-centered configurations at 723 K present the octahedral structures. According to Fig. 3 and Fig. 4, the bond-angle relations of Ge-centered and Sb-centered structures vary notably with temperature while the coordination environments of them change relative little. Then it is inferred that the structural orders of Ge-centered and Sb-centered configurations dominantly depend on the adjustment of bond-angle relation, rather than the variation of CNs. The Te-centered configuration at 723 K is still relative disordered, it is probably due to the even low CN of Te atom.

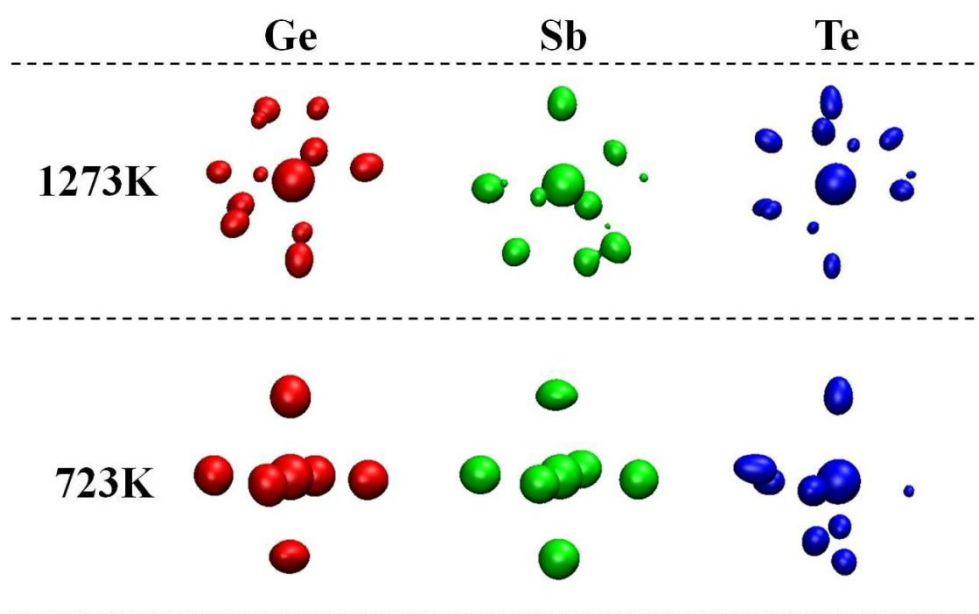


Fig. 5 The collective alignments results of Ge-centered (red), Sb-centered (green) and Te-centered (blue) clusters for GST326 at 1273 K and 723 K. The isovalue is set at 0.2 \AA^{-3} .

In addition to the BADF identifying the orderliness by angle, now an individual

cluster-template alignment from ACA analysis⁴⁸ which can identify the structural order by bond length, is used to explore the evolution of the octahedrons with temperature. As seen in snapshot from Fig. 6(a), a standard 3-fold defective octahedron is selected as the template for individual cluster-template alignment, due to it is not only the basis unit of octahedron, but also the mainly component in supercooled liquid GST326. In an individual cluster-template alignment, the standard 3-fold octahedron is fixed, then the selected single cluster is randomly rotated to minimize the mean-square distance to the template. A parameter called “structure fitting score f ” can be used to describe the structural similarity of selected cluster to the template,

$$\Delta r_T^2 = \min_{C=1,\dots,n_C} \Delta r_{C,T}^2 \quad (4)$$

$$f = \min \left(\frac{1}{n_T} \sum_{T=1}^{n_T} \Delta r_T^2 \right) \quad (5)$$

where $\Delta r_{C,T}^2$ represents the distance between atom C in cluster and atom T in template. Δr_T^2 is the minimal square distance between atom T in the template and all n_C atoms in selected cluster. $f=0$ means that the selected cluster is same to the template, while a larger f indicates that the selected cluster deviates more to the template.

The results of individual cluster-template alignment are shown in Fig. 6. Fig. 6(a)-(c) depict the distributions of fitting scores of Ge-centered, Sb-centered and Te-centered clusters at different temperatures, respectively. At 1273 K, the fitting scores for the three configurations distribute in a large range, indicating that there are many clusters deviated from the standard 3-fold octahedron. As the temperature gradually decreases to 723 K, more and more fitting scores are shifting close to zero, illustrating that many disordered configurations tend to form the more ordered defective octahedrons when GST326 is cooled from a liquid to a supercooled liquid.

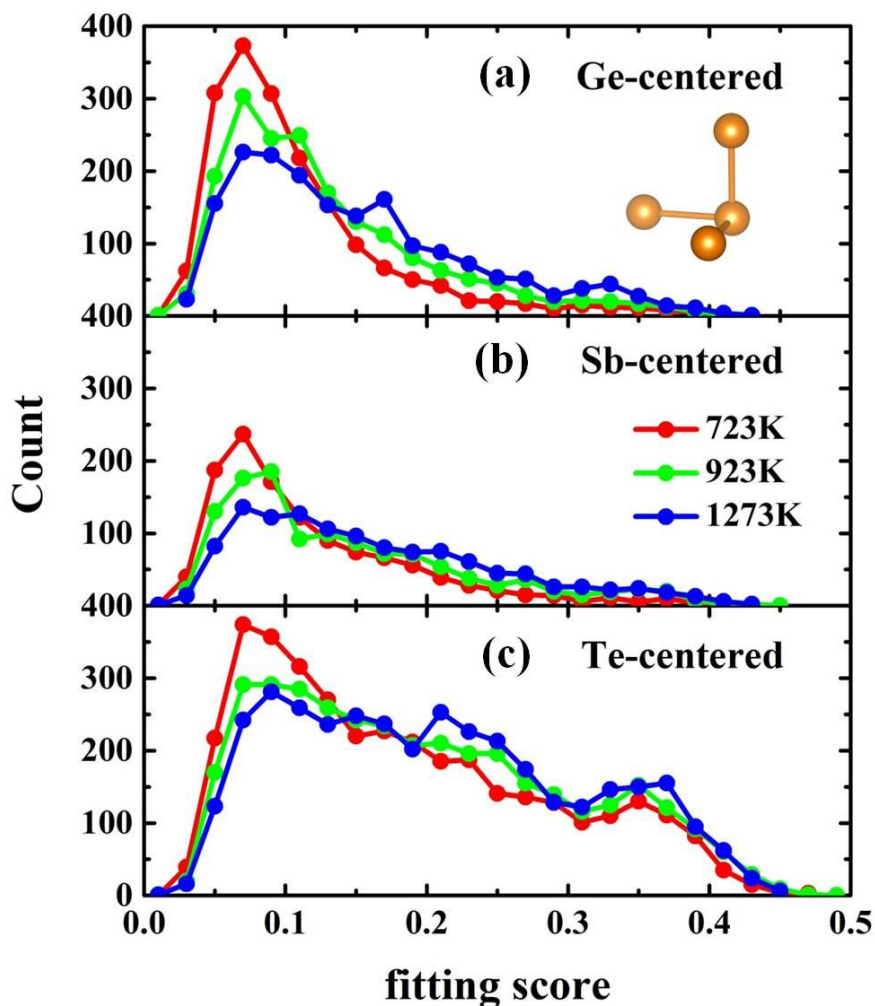


Fig. 6 Distributions of fitting scores of (a) Ge-centered, (b) Sb-centered and (c) Te-centered configurations at different temperatures. The standard 3-fold octahedron (snapshot in (a)) is used as the template for cluster-template alignment.

In previous studies^{8, 12, 46, 49}, it is reported that amorphous Ge-Sb-Te compounds are usually composed of a large fraction of defective octahedrons and a small portion of Ge-centered tetrahedrons. Thus it is necessary to explore the change of tetrahedron in the cooling process. The local structural order parameter q is an effective tool to identify the tetrahedrons in the liquid and amorphous systems⁵⁰⁻⁵¹, which can be expressed as

$$q = 1 - \frac{3}{8} \sum_{i>k} \left(\frac{1}{3} + \cos \theta_{ijk} \right)^2 \quad (6)$$

where the sum runs over the couples of atoms bonded to a central atom j . $q=1.0$

represents the ideal tetrahedral geometry, and then the fraction of tetrahedrons can be identified by an integration from 0.8 to 1.0. Fig. 7(a) shows the distributions of q at different temperatures. As the temperature decreases, more q values shift to 1.0, leading to an increase in the fraction of tetrahedron, as shown in Fig. 7(b). Then it is clear that tetrahedrons originate from the liquid, and increase at a lower temperature. Due to the stable CN of Ge atom, the increasing tetrahedrons may be formed by the arrangement of neighboring atoms.

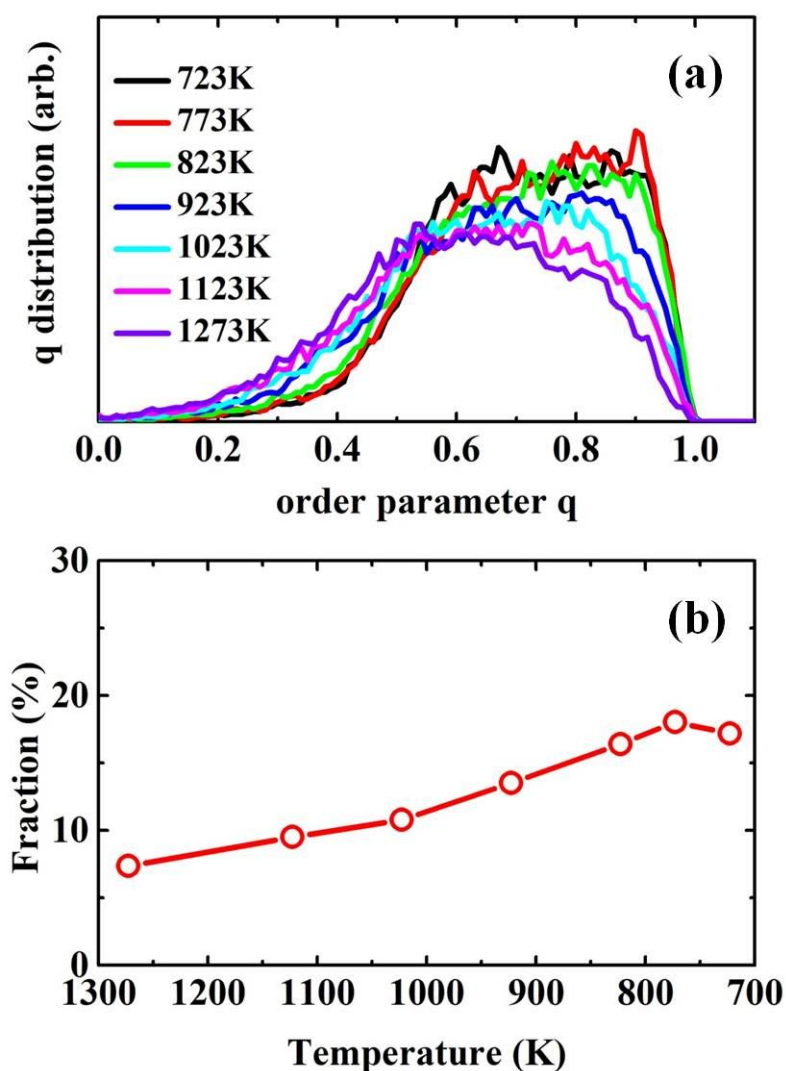


Fig. 7 (a) Distribution of the local order parameter q for four-coordinated Ge-centered clusters. (b) Fraction of tetrahedron in Ge-centered clusters with temperature.

Primitive ring analysis is a useful tool to character the MRO in the liquid systems⁵². By using RINGS code⁵³, Fig. 8(a) and (b) count the distributions of

primitive rings in GST326 at 1273 K and 723 K, respectively. 4-fold rings, as a signature of MRO in liquid, are pointed out to be the basic structural elements for fast phase transition in PCMs^{17, 31, 54}. Thus variation of 4-fold rings can reflect the origin of MRO in supercooled liquid GST326. At 1273 K, 3-fold, 4-fold and 5-fold rings possess a very large proportion, the largest fraction of 3-fold ring suggests that the strong localization of local configurations. At 723 K, the fraction of 3-fold rings decreases obviously while that of 4-fold rings becomes to the largest one, illustrating that the MROs arise in the supercooled liquid GST326. In our previous studies, it is found that 4-fold rings are mainly formed by the connectivity of octahedrons²³, and octahedrons can provide many sites for the formation of 4-fold rings¹². Then it is expected that the increase of 4-fold rings in supercooled liquid GST326 is dominantly induced by the enhancement of orderliness in defective octahedrons. This is because that planar 4-fold ring can effectively reduce the interfacial energy between the ordered and disordered sections¹⁷. Thus, these more ordered defective octahedrons formed in the fast cooling process are believed to be the origin of MRO in PCMs.

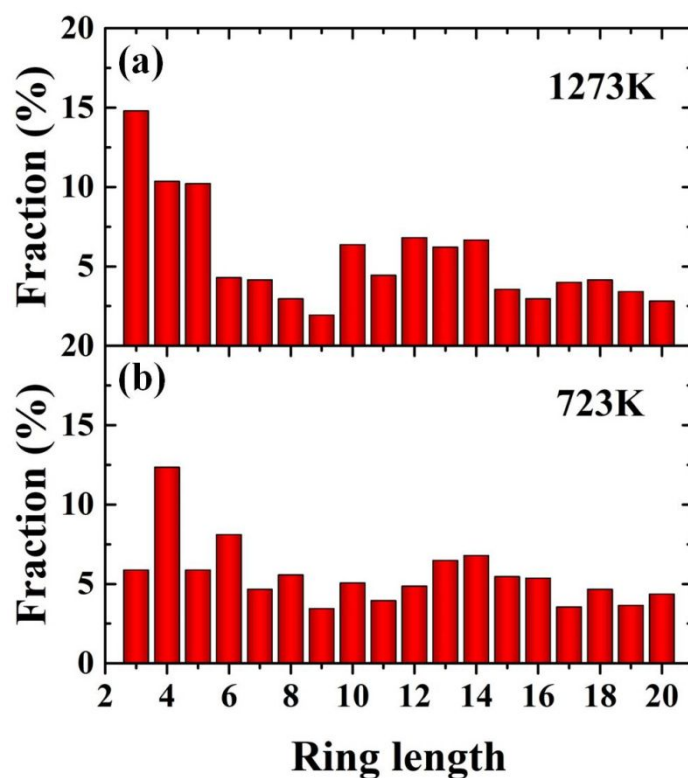


Fig. 8 Distributions of primitive ring for GST326 at (a) 1273 K and (b) 723 K, respectively.

To investigate the influence of structural changes on electronic properties, the electronic density of states (DOS) at different temperatures are calculated, as shown in Fig. 9. Fig. 9(a) plots total DOS of GST326 varying with the temperature. Similar to the previous study²², a pseudogap at the vicinity of zero is also observed, and it continues to open as the temperature decreases. To further study the tendency, Figs. 9(b) and (c) present the projected DOS of Ge, Sb and Te atoms at 1273 and 723 K, respectively. At 1273 K, the pseudogap is dominantly composed of Ge-p, Sb-p and Te-p states, in which Ge-p shows a pseudogap at the vicinity of Fermi energy, Sb-p state is the smallest one while Te-p state is the largest one. As the temperature decreases to 723 K, the Ge-p state at ~ 0 eV reduces notably and becomes the smallest one, the Sb-p state reduces relative little, while the Te-p state reduces obviously but remains the largest one. This is because that the Ge-centered configurations become more ordered in the cooling process (as shown in Fig. 3), these more ordered clusters are closer to the local structures in crystal, leading to the expansion of pseudogap. The small drop of Sb-p state may ascribe to the smaller structural change of Sb-centered cluster than those of Ge- and Te-centered clusters, as there is a sign of pseudogap at 723 K. The remaining Sb-state may be induced by the Sb-Sb bonding, because CN of Sb-Sb configuration changes little during the cooling process (as shown in Fig. 4(b)). The prominent pseudogap of Te-p state at 723 K is also due to the enhancement of structural order. The Te-p state is always the largest one in the cooling process, it is probably that the Te-centered clusters are relative disorder when comparing with Ge- and Sb-centered clusters (as shown in Fig. 5). Then it is clear that the pseudogap opening tendency mainly originates from the enhancement of structural order under cooling.

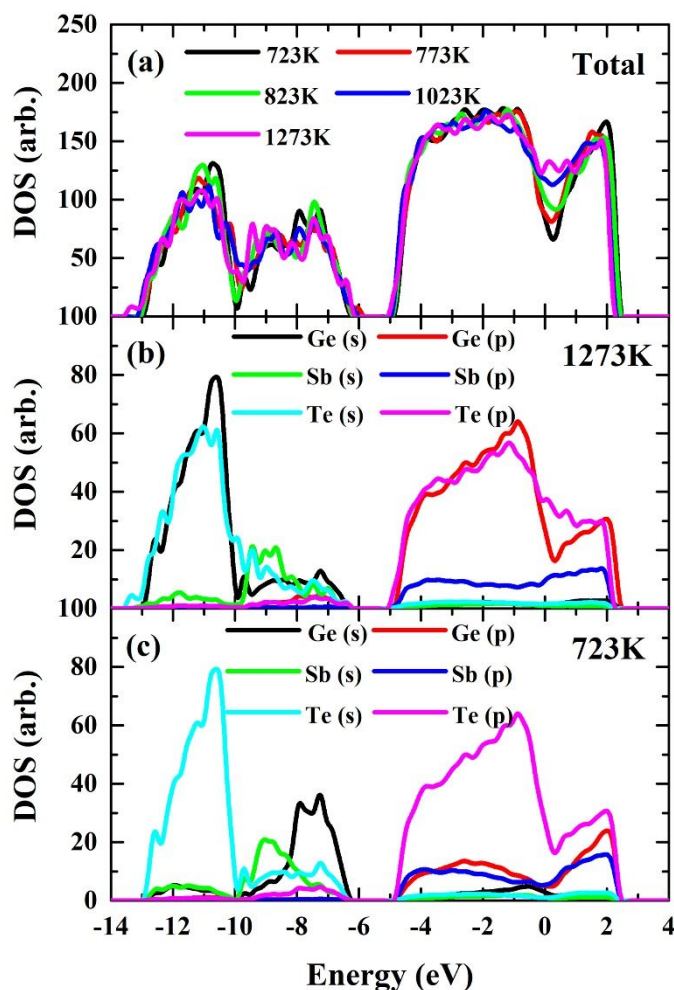


Fig. 9 (a) Total DOS of GST326 at different temperatures, and projected DOS of GST326 at (b) 1273 K and (c) 723 K, respectively.

Conclusions

In summary, the AIMD simulations were performed to investigate the structural evolution as GST326 was fast cooled from a liquid to a supercooled liquid. Throughout the cooling process, though CNs of homopolar bonding configurations decrease and those of heteropolar bonding cases increase, total CNs of Ge, Sb and Te change very little, suggesting that local configurations in supercooled liquid keep the coordination environment from the liquid, but present more chemical homogeneous. By using the BADF and ACA methods, it is found that the short-range structures change to the more ordered defective octahedrons dominantly by adjusting of bond-angle relation and bond length. Furthermore, the MRO is observed in the

supercooled liquid stage, accompanying with the enhancement of structural orders of defective octahedrons. Then it is expected that the more ordered defective octahedrons are the origin of structural order in PCMs. These findings offer us a deep insight on the origins of SRO and MRO in supercooled liquid GST326, which is of great importance for further understanding of the phase-change mechanism in PCMs.

Acknowledgments

This work was supported by the National Natural Science Foundation of China (Grant Nos. 11504332, 61427815 and 11374055), the Key Projects of Basic Research of the Shanghai Municipal Science and Technology Commission (No. 18JC1411500), and the Fudan High-end Computing Center. The work at Ames Laboratory was supported by the U.S. Department of Energy, Basic Energy Sciences, and Division of Materials Science and Engineering, including a grant of computer time at the National Energy Research Scientific Computing Centre (NERSC) in Berkeley, CA. Ames Laboratory is operated for the U.S. DOE by Iowa State University under Contract No. # DE-AC02-07CH11358.

References

1. A. Pirovano, A. L. Lacaita, A. Benvenuti, F. Pellizzer and R. Bez, *IEEE Trans. Electron. Dev.*, 2004, **51**, 452-459.
2. R. Bez and A. Pirovano, *Mat. Sci. Semicon. Proc.*, 2004, **7**, 349-355.
3. M. Wuttig and N. Yamada, *Nat. Mater.*, 2007, **6**, 824-832.
4. G. Atwood, *Science*, 2008, **321**, 210-211.
5. A. L. Lacaita and D. J. Wouters, *Phys. Status Solidi A*, 2008, **205**, 2281-2297.
6. S. Raoux, G. W. Burr, M. J. Breitwisch, C. T. Rettner, Y. C. Chen, R. M. Shelby, M. Salinga, D. Krebs, S. H. Chen, H. L. Lung and C. H. Lam, *IBM J. Res. Dev.*, 2008, **52**, 465-479.
7. W. Welnic and M. Wuttig, *Mater. Today*, 2008, **11**, 20-27.
8. S. Caravati, M. Bernasconi, T. D. K hne, M. Krack and M. Parrinello, *Appl. Phys. Lett.*, 2007, **91**, 171906.
9. P. Jovari, I. Kaban, J. Steiner, B. Beuneu, A. Schoeps and M. A. Webb, *Phys. Rev. B*, 2008, **77**, 035202.
10. M. Krbal, A. V. Kolobov, P. Fons, J. Tominaga, S. R. Elliott, J. Hegedus and

- T. Uruga, *Phys. Rev. B*, 2011, **83**, 054203.
11. C. Qiao, Y. R. Guo, F. Dong, J. J. Wang, H. Shen, S. Y. Wang, M. Xu, X. S. Miao, Y. X. Zheng, R. J. Zhang, L. Y. Chen, C. Z. Wang and K. M. Ho, *J. Mater. Chem. C*, 2018, **6**, 5001-5011.
 12. C. Qiao, Y. R. Guo, J. J. Wang, H. Shen, S. Y. Wang, Y. X. Zheng, R. J. Zhang, L. Y. Chen, C. Z. Wang and K. M. Ho, *J. Alloys Compd.*, 2019, **774**, 748-757.
 13. T. Nonaka, G. Ohbayashi, Y. Toriumi, Y. Mori and H. Hashimoto, *Thin Solid Films*, 2000, **370**, 258-261.
 14. T. Matsunaga, N. Yamada and Y. Kubota, *Acta Crystallogr. B*, 2004, **60**, 685-691.
 15. Z. M. Sun, J. Zhou and R. Ahuja, *Phys. Rev. Lett.*, 2006, **96**, 055507.
 16. K. Shportko, S. Kremers, M. Woda, D. Lencer, J. Robertson and M. Wuttig, *Nat. Mater.*, 2008, **7**, 653-658.
 17. T. H. Lee and S. R. Elliott, *Phys. Rev. Lett.*, 2011, **107**, 145702.
 18. M. Krbal, A. V. Kolobov, P. Fons, J. Tominaga, S. R. Elliott, J. Hegedus, A. Giussani, K. Perumal, R. Calarco, T. Matsunaga, N. Yamada, K. Nitta and T. Uruga, *Phys. Rev. B*, 2012, **86**, 045212.
 19. J. Orava, A. L. Greer, B. Gholipour, D. W. Hewak and C. E. Smith, *Nat. Mater.*, 2012, **11**, 279-283.
 20. C. Qiao, Y. R. Guo, J. J. Wang, H. Shen, S. Y. Wang, Y. X. Zheng, R. J. Zhang, L. Y. Chen, C. Z. Wang and K. M. Ho, *J. Non-Cryst. Solids*, 2019, **503**, 382-388.
 21. G. C. Sosso, J. Colombo, J. Behler, E. Del Gado and M. Bernasconi, *J. Phys. Chem. B*, 2014, **118**, 13621-13628.
 22. P. Zalden, F. Quirin, M. Schumacher, J. Siegel, S. Wei, A. Koc, M. Nicoul, M. Trigo, P. Andreasson, H. Enquist, M. J. Shu, T. Pardini, M. Chollet, D. Zhu, H. Lemke, I. Ronneberger, J. Larsson, A. M. Lindenberg, H. E. Fischer, S. Hau-Riege, D. A. Reis, R. Mazzarello, M. Wuttig and K. Sokolowski-Tinten, *Science*, 2019, **364**, 1062-1067.
 23. Y. R. Guo, F. Dong, C. Qiao, J. J. Wang, S. Y. Wang, M. Xu, Y. X. Zheng, R. J. Zhang, L. Y. Chen, C. Z. Wang and K. M. Ho, *Phys. Chem. Chem. Phys.*, 2018, **20**, 11768-11775.
 24. S. Caravati, M. Bernasconi and M. Parrinello, *Phys. Rev. B*, 2010, **81**, 014201.
 25. B. Sa, J. Zhou, Z. Sun, J. Tominaga and R. Ahuja, *Phys. Rev. Lett.*, 2012, **109**, 096802.
 26. T. Matsunaga and N. Yamada, *Phys. Rev. B*, 2004, **69**, 104111.
 27. A. Klein, H. Dieker, B. Spaeth, P. Fons, A. Kolobov, C. Steimer and M. Wuttig, *Phys. Rev. Lett.*, 2008, **100**, 016402.
 28. M. Xu, W. Zhang, R. Mazzarello and M. Wuttig, *Adv. Sci.*, 2015, **2**, 1500117.
 29. I. Friedrich, V. Weidenhof, W. Njoroge, P. Franz and M. Wuttig, *J. Appl. Phys.*, 2000, **87**, 4130-4134.
 30. B. S. Lee, J. R. Abelson, S. G. Bishop, D. H. Kang, B. K. Cheong and K. B. Kim, *J. Appl. Phys.*, 2005, **97**, 093509.

31. J. Hegedus and S. R. Elliott, *Nat. Mater.*, 2008, **7**, 399-405.
32. J. Akola and R. O. Jones, *Phys. Rev. B*, 2007, **76**, 235201.
33. J. Y. Raty, W. Zhang, J. Luckas, C. Chen, R. Mazzarello, C. Bichara and M. Wuttig, *Nat. Commun.*, 2015, **6**, 7467.
34. V. L. Deringer, W. Zhang, M. Lumeij, S. Maintz, M. Wuttig, R. Mazzarello and R. Dronskowski, *Angew. Chem. Int. Edit.*, 2014, **53**, 10817-10820.
35. J. E. Boschker, M. Boniardi, A. Redaelli, H. Riechert and R. Calarco, *Appl. Phys. Lett.*, 2015, **106**, 023117.
36. B. Sa, N. Miao, J. Zhou, Z. Sun and R. Ahuja, *Phys. Chem. Chem. Phys.*, 2010, **12**, 1585-1588.
37. J. L. F. Da Silva, A. Walsh and H. Lee, *Phys. Rev. B*, 2008, **78**, 224111.
38. T. Matsunaga, R. Kojima, N. Yamada, K. Kifune, Y. Kubota and M. Takata, *Appl. Phys. Lett.*, 2007, **90**, 161919.
39. F. Rao, W. Zhang and E. Ma, *Science*, 2019, **364**, 1032-1033.
40. Kresse and Hafner, *Phys. Rev. B*, 1993, **47**, 558-561.
41. Kresse and Furthmuller, *Phys. Rev. B*, 1996, **54**, 11169-11186.
42. Blochl, *Phys. Rev. B*, 1994, **50**, 17953-17979.
43. J. P. Perdew, K. Burke and M. Ernzerhof, *Phys. Rev. Lett.*, 1996, **77**, 3865-3868.
44. A.-K. U. Michel, P. Zalden, D. N. Chigrin, M. Wuttig, A. M. Lindenberg and T. Taubner, *ACS Photonics*, 2014, **1**, 833-839.
45. E.-R. Sittner, K. S. Siegert, P. Jost, C. Schlockermann, F. R. L. Lange and M. Wuttig, *Phys. Status Solidi A*, 2013, **210**, 147-152.
46. Z. Sun, J. Zhou, A. Blomqvist, B. Johansson and R. Ahuja, *Appl. Phys. Lett.*, 2008, **93**, 061913.
47. H. Weber, M. Schumacher, P. Jovari, Y. Tsuchiya, W. Skrotzki, R. Mazzarello and I. Kaban, *Phys. Rev. B*, 2017, **96**, 054204.
48. X. W. Fang, C. Z. Wang, Y. X. Yao, Z. J. Ding and K. M. Ho, *Phys. Rev. B*, 2010, **82**, 184204.
49. M. Upadhyay, S. Murugavel, M. Anbarasu and T. R. Ravindran, *J. Appl. Phys.*, 2011, **110**, 083711.
50. J. R. Errington and P. G. Debenedetti, *Nature*, 2001, **409**, 318-321.
51. A. Bouzid, G. Ori, M. Boero, E. Lampin and C. Massobrio, *Phys. Rev. B*, 2017, **96**, 224204.
52. W. Zhang, R. Mazzarello, M. Wuttig and E. Ma, *Nat. Rev. Mater.*, 2019, **4**, 150-168.
53. S. Le Roux and P. Jund, *Comput. Mater. Sci.*, 2010, **49**, 70-83.
54. F. Rao, K. Ding, Y. Zhou, Y. Zheng, M. Xia, S. Lv, Z. Song, S. Feng, I. Ronneberger, R. Mazzarello, W. Zhang and E. Ma, *Science*, 2017, **358**, 1423-1426.